DOI: 10.1002/ejic.200900866

Controllable Synthesis of Cu_2O Microcrystals via a Complexant-Assisted Synthetic Route

Wanqun Zhang,[a,b] Lei Shi,*[a] Kaibin Tang,[a,b] and Shumei Dou[b]

Keywords: Synthesis design / Crystal growth / Microcages / Photochemistry / Hydrothermal synthesis

A novel method using $Cu(AC)_2{\cdot}H_2O$ and dimethylglyoxime as reagents has been successfully developed for the controllable synthesis of Cu_2O microcrystals with distinctive morphologies, including porous hollow microspheres, octahedral microcages, and microcrystals with truncated corners and edges and octahedral microcrystals. These structures can be fine-tuned by varying reaction temperature, reaction time, and concentration. The products were characterized by X-ray diffraction, field emission scanning electron microscopy, X-ray photoelectron spectra, and UV/Vis diffuse reflectance spectra. This is the first report of the preparation of the novel microcage structure of Cu_2O through a simple solution-based route. By investigating the intermediate products which resemble the final crystal structures, a possible growth mechanism is proposed. Moreover, the investigations showed that the various 3D architectures of the as-made products exhibit different abilities to catalytically degrade rhodamine-B. Our work shows that octahedral Cu_2O crystals with entirely {111} faces are photocatalytically more active than octahedral microcrystals with truncated corners and edges, suggesting the {111} faces of Cu_2O nanostructures are catalytically more active than the {100} and {110} faces. Due to dual effect of the cavity structure and the {111} surfaces, the octahedral microcages with truncated corners and edges exhibit a higher extent of the photodecomposition reaction. As a result of very slow photocorrosion rate of the Cu_2O microcrystal, it is expected that these microcrystals with different surfaces may find more applications in photocatalysis.

Introduction

During the past few decades, much attention has been focused on inorganic materials with a specific size and structure of their outer shape due to their fundamental significance in investigating the dependence of various physical properties on structure and size reduction, as well as their potential applications in many fields. In recent years, there have been an increasing number of studies on the synthesis of novel semiconductor materials with different structures including cubes,[1] rods,[2,3] belts,[4,5] plates,[6] hollow spheres,[7,8] and wires.[9,10]

As an important *p*-type semiconductor material, Cu_2O is a promising material with potential applications in solar energy conversion,[11,12] catalysis for organic reactions,[13,14] electrode material for lithium ion batteries, biosensor and magnetic storage devices,[15–17] and gas sensors.[18] Cu_2O has been found to be a stable photocatalyst for the photochemical decomposition of water into O_2 and H_2 under visible-light irradiation.[19] Furthermore, Cu_2O crystals have been a center for the study of Bose–Einstein condensation (BEC) of excitons.[20] To date, different structures such as octahedral, cages, nanocubes, and nanoboxes have been synthesized. Cu_2O octahedral micro- and nanocrystals were prepared successfully in Triton X-100 W/O microemulsions under γ-irradiation and in the presence of glucose, respectively.[21,22] Hydrothermal preparation of hexapod-like Cu_2O whiskers have also been reported.[23] In the presence of glucose, octahedral Cu_2O nanocages having an edge length of 230 nm were obtained by using a catalytic self-templating route.[24] Murphy and Gou reported the solution-phase synthesis of highly monodisperse Cu_2O nanocubes by employing cetyltrimethylammonium bromide (CTAB) as the protecting reagent.[25] Using hydrazine monohydrate as a reducing agent, Cu_2O nanoboxes with hollow interiors were prepared through the formation of Cu_2O nanocubes from copper ions in aqueous acetic acid solution.[26] Cu_2O nanospheres have been synthesized in the absence of templates and additives by the hydrothermal method by using $Cu(CH_3COO)_2{\cdot}H_2O$ as a precursor or by heating a solution of copper acetate and hydrazine as the reductant in 2-propanol under reflux conditions.[27,28] Recently, Kuo et al. reported a simple approach for the fabrication of cuprous oxide (Cu_2O) nanocages and nanoframes possessing an unusual truncated rhombic dodecahedral structure.[29]

Although several successful synthetic strategies have been demonstrated for the preparation of Cu_2O materials with different sizes and shapes, they should be carried out under

[a] Hefei National Laboratory for Physical Sciences at Microscale, University of Science and Technology of China, Hefei, Anhui 230026, Republic of China
Fax: +86-551-3607924
E-mail: shil@ustc.edu.cn
[b] Department of Chemistry, University of Science and Technology of China, Hefei, Anhui 230026, China

some special conditions, such as at high temperature, in multistep sample preparation processes, and/or with the use of templates, polymers, and surfactants, and so on. Up to now, developing facile, mild, easily controlled, and template-free methods to create novel patterns on self-generated homogeneous substrates is still required. In this paper, we report a low-temperature hydrothermal route without a preformed template to prepare Cu_2O crystallites with controlled morphologies, including porous hollow microspheres, octahedral microcages and microcrystals with truncated corners and edges and octahedral microcrystals. To the best of our knowledge, this is the first, one-step, solution-based synthesis of novel octahedral microcages with truncated corners and edges. In particular, a process mechanism has been revealed for the growth of these kinds of Cu_2O microcrystals. Cu_2O microparticles, whose photocorrosion rate is very slow, have a higher photocatalytic activity than Cu_2O nanoparticles, although Cu_2O microparticles have much lower adsorption capacity than Cu_2O nanoparticles. As a result, the photocatalytic properties of the Cu_2O microcrystals are also presented.

Results and Discussion

It is well know that dimethylglyoxime is a good linker ligand, which can form $Cu(Hdmg)_2$ (Hdmg = dimethylglyoxime anion) with Cu^{2+} in alkaline condition. The reaction in the present system first forms Cu–dimethylglyoxime complexes, and then the complexes yield NH_2OH upon hydrolysis [Scheme 1, Equations (1) and (2)]. It is expected that $Cu(OH)_4^{2-}$ ions are formed readily upon the addition of NaOH and reduced to Cu_2O by NH_2OH [Scheme 1, Equations (3)].

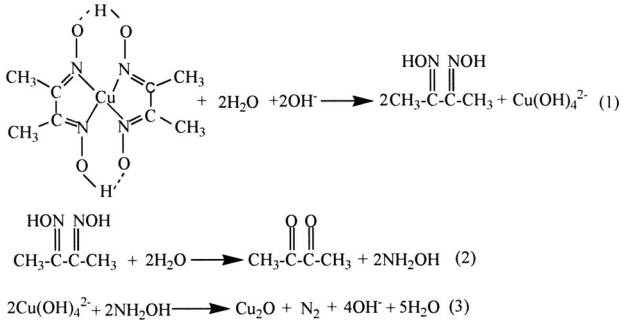

Scheme 1.

To investigate the reaction mechanism, the finished reaction solution was analyzed. Ultraviolet spectrophotometry was used to determine 2,3-butanedione in the finished reaction solution with *o*-diaminobenzene hydrochloride as apparent color agent under 335 nm detection wavelength.[30] The result (Figure 1) reveals the presence of 2,3-butanedione in the finished reaction solution, which is supportive to the reaction above.

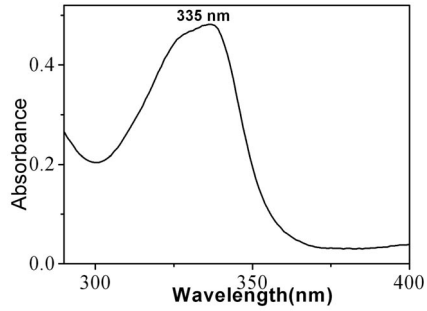

Figure 1. Absorption spectra of the interaction systems of the finished reaction solution and *o*-diaminobenzene hydrochloride.

Figure 2 shows the XRD patterns of the as-prepared Cu_2O particles synthesized at different NaOH concentrations from 0.23 to 0.91 M. All the diffraction peaks can be indexed as cubic-phase Cu_2O. The calculated cell constants of the three products are a_1 = 4.29 Å, a_2 = 4.28 Å, and a_3 = 4.29 Å, which agree well with that of the literature (JCPDS 05–0667, a = 4.269 Å). It is noticed that the intensities of the peaks in Figure 2a are consistent with the literature. However, in Figure 2c, the related intensity of the (111) reflection is much stronger than that of the standard powder diffraction pattern, which may suggest the existence of preferential orientation due to the special shape of the microcrystals. From Figure 2a, on the basis of the Debye–Scherrer formula, the average grain size of the product along the [111] direction is about 31.2 nm.

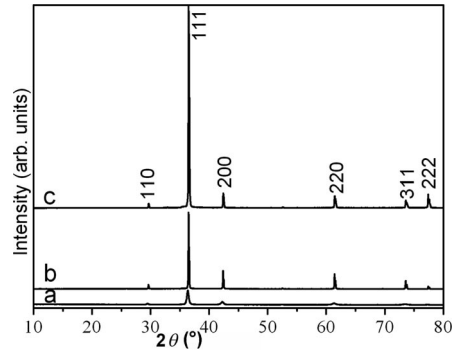

Figure 2. XRD pattern of the Cu_2O particles prepared with $[Cu(AC)_2 \cdot H_2O]$ = 0.025 M, $[dmgH_2]$ = 0.05 M, and NaOH with concentrations of (a) 0.23 M, (b) 0.45 M, and (c) 0.91 M at 150 °C for 20 h, respectively.

The yield of Cu species is counted from the added amount of $Cu(AC)_2 \cdot H_2O$; the yields of Cu species prepared with different NaOH concentrations (0.23, 0.45, and 0.91 M) are 96, 95, and 90%, respectively. The morphology of the product was determined by FE-SEM. Typical SEM images of Cu_2O microcrystals prepared with different NaOH concentrations are shown in Figures 3 and 4. Obviously, the morphology of Cu_2O crystallite can be tailored by adjusting the NaOH concentration, which is filled into the autoclave. When the NaOH concentration is 0.23 M, porous hollow microspheres with a diameter of about 5–9 μm dominate the products (Figure 3a,b). On the basis of the

SEM images at different magnifications, it is found that the pores are distributed on the surfaces of the microspheres (Figure 3b). Through the image of the broken microsphere, which provides an opportunity to see the "open" structure, the hollow nature of the spheres is confirmed by the typical FE-SEM image (Figure 3b, inset). A close inspection of these structures identifies that the porous hollow microspheres usually are made up of rod-like crystallites radiating from the center. When the NaOH concentration is increased to 0.45 M, some novel structures of microcages are observed (Figure 3c,d). These microcages have a diameter of about 6–7 μm. A careful observation confirms their octahedral structure with truncated corners and edges (Figure 3d). The image of broken microcages reveals their hollow interiors (Figure 3d, inset). Figure 4 shows SEM images of the microcages viewed along the <100>, <111>, and <110> directions. Each microcage contains eight {111} faces with holes, six {100} faces, and eight leaf-like curved faces. On increasing the NaOH concentration to 0.91 M, perfect octahedra with a size of 6–7 μm could be obtained (Figure 3e).

The above-mentioned results indicate that, in our aqueous system, the starting NaOH concentration shows a strong effect on the formation of the final morphology of Cu_2O crystallites. Generally, the growth process of crystals can be separated into two steps, an initial nucleating stage and a subsequent crystal growth process. At the initial nucleating stage, the crystalline phase of the seeds is critical for directing the intrinsic shapes of the crystals due to its characteristic symmetry and structure. At the subsequent step, the crystal growth stage is a kinetically and thermodynamically controlled process that can yield more complicated shapes with some degree of shape tenability through changing the reaction parameters such as temperature, reaction time, concentration, PH value, and so on.[31–34] As a result, one can control the growth of the crystal by controlling the processing conditions based on the intrinsic properties of the crystal. To investigate the formation mechanism of Cu_2O growth of porous microspheres and microcages in our aqueous system, the products formed at various stages of the growth process were examined. Figure 5 displays the intermediate Cu_2O microcrystals obtained with different starting NaOH concentrations at 150 °C. At the beginning of the reaction, under supersaturated conditions, a burst of Cu_2O nucleation is formed mainly by a kinetic growth regime in the initial concentrated synthetic solution, because the solubility product of Cu_2O is rather small in the present solution. With the nucleation and growth of Cu_2O, a large amount of ultra-small Cu_2O nanoparticles is formed due to the high flux of monomers. These nanoparticles quickly aggregate in order to reduce the overall energy of the system and form spheres within about 60 min of the reaction (Figure 5a,e). When the NaOH concentration was 0.23 M, microspheres with rough surfaces appear. With a prolonged reaction time, the particles on the surface of the sphere become larger and larger, indicating that rapid crystal growth has occurred (Figure 5b). Meanwhile, fewer OH^- ions could be adsorbed on the Cu_2O surface due to the relatively low concentration of

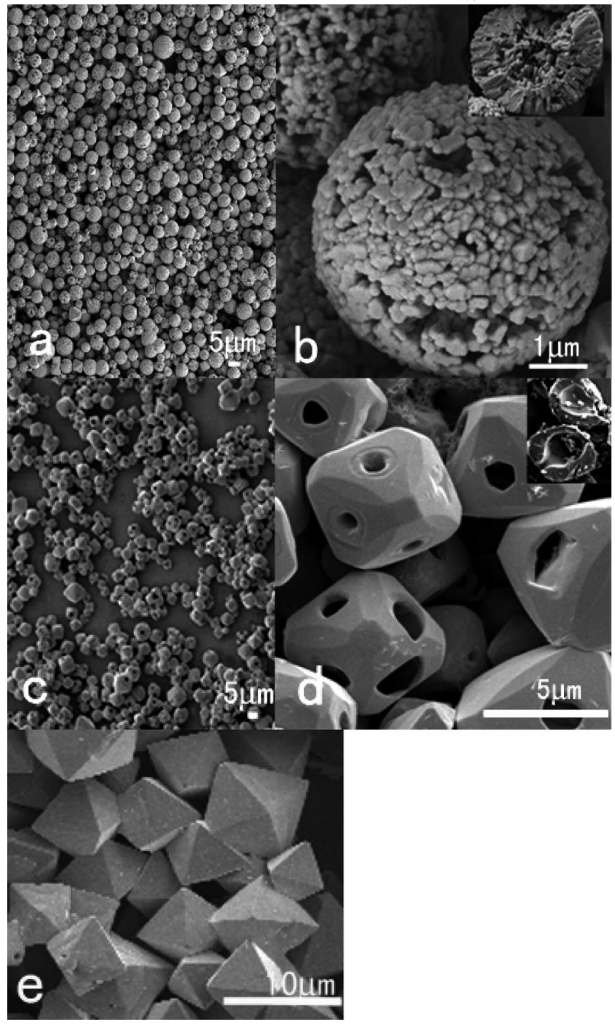

Figure 3. SEM images of Cu_2O crystallites prepared hydrothermally with $[Cu(AC)_2{\cdot}H_2O]$ = 0.025 M, $[dmgH_2]$ = 0.05 M, and NaOH with concentrations of (a,b) 0.23 M, (c,d) 0.45 M, and (e) 0.91 M at 150 °C for 20 h. Insets of b and d are the "open" structures of the microcrystals.

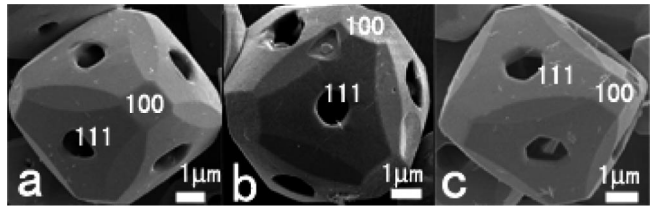

Figure 4. SEM images of single microcage viewed along the (a) <100>, (b) <111>, and (c) <110> directions.

OH^-, leading to the formation of spherical particles without preferential growth on certain facets. The crystallite agglomeration was then followed by a solid core evacuation,[35,36] as shown in Figure 5b,c. The formation of the hollow spheres can be understood by a recrystallization process (i.e., Ostwald ripening) of the microspheres of Cu_2O in the core evacuation. In Figure 5c, the void space in the Cu_2O microspheres gets bigger with age, which results because the smaller crystallites located at the central cores

have higher surface energy and they tend to relocate themselves to the shell parts during Ostwald ripening. After aging the reaction, the crystallites in the shell become larger and larger, which results in the formation of a porous structure. Varying the pH value, to a certain extent, would change the growth rate of the crystallographic planes with different surface energies so as to form different crystallite morphologies.[37–42] When the NaOH concentration is 0.45 M, on the other hand, the nucleation rate of Cu_2O decreased in highly concentrated alkaline solutions. A supersatured solution of Cu^+ ions could provide enough Cu^+ ions for preferential growth. The seed particles continuously adsorb onto these intermediate structures to allow further growth, and then disordered nanoparticle aggregates approximating the shape of octahedra were observed (Figure 5f,g). The aggregates with rough surfaces suggest a morphology resembling that of an octahedron can be formed via the aggregation of individual smaller particles on the surface of the spheres (Figure 5f). Similarly, these microcrystals underwent a solid core evacuation (Figure 5h, inset). Murphy et al. reported that the preferential adsorption of molecules and ions in solution to different crystal faces makes the nanoparticles develop into various shapes by controlling the growth rates along different crystal axes.[43] Moreover, the shape of the fcc crystal was mainly dominated by the ratio of the growth rate in the <100> direction to that in the <111> direction, which is usually defined as the value of *R*. When *R* is 1.15 and 1.73, truncated octahedral and perfect octahedral particles are obtained.[44] From the above analysis, it is found that the NaOH concentration may give an evident effect on the growth rate along the [100] direction relative to that of the [111] direction. The intermediate structures then evolve into structurally well-defined final products via a surface reconstruction process (Figure 5g–i). Interestingly, there are holes on some panels of the cages. This can be attributed to the fact that the limited NaOH content cannot supply enough Cu_2O monomer to produce nanoparticles in the process of surface reconstruction so that {111} faces are filled incompletely. Therefore, with an increase in NaOH concentration (0.91 M), perfect octahedra with a size of 6–7 μm can be fabricated (Figure 3e).

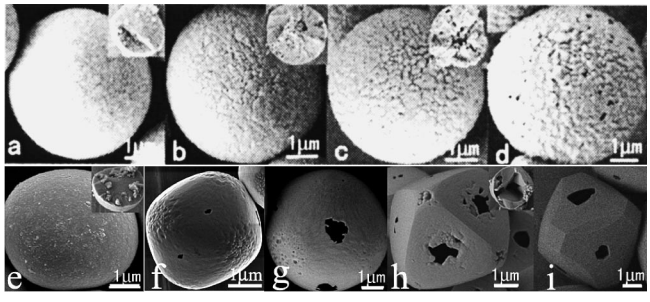

Figure 5. FE-SEM images of samples prepared with $[Cu(AC)_2 \cdot H_2O]$ = 0.025 M, $[dmgH_2]$ = 0.05 M, and [NaOH] = 0.23 M at 150 °C for reaction times of (a) 1 h, (b) 2 h, (c) 3 h, and (d) 4 h; the intermediate crystals captured after aging the reaction for (e) 1 h, (f) 1.5 h, (g) 2 h, (h) 3 h, and (i) 4 h with [NaOH] = 0.45 M. The insets are the "open" structures of the microcrystals.

Reaction temperature also affects the morphology of the products. Typical SEM images of Cu_2O microcrystals prepared at different temperatures are shown in Figure 6. When the reaction is conducted with 0.23 M NaOH at 180 and 200 °C, the microcrystal morphologies remain the same as those of 150 °C, except a few of the pores distribute on the surface due to the increase in the crystallite size of the surface particles. When the reaction temperature is increased from 150 to 180 °C while keeping the NaOH concentration at 0.45 M and other synthetic conditions unchanged, octahedral microcrystals with truncated corners and edges are obtained. The microcrystals are 6–7 μm in diameter. Each microcrystal contains 6 octagonal {100} faces, 8 truncated triangular {111}, and 12 quadrate {110} faces (Figure 6a). With an increase in the reaction temperature, microcrystals may go through secondary growth, which is in favor of the growth of perfect crystals. When the reaction was conducted at 200 °C, {110} faces become rough and increase their width, but {100} faces partly evolve into round (Figure 6b). Therefore, it can be concluded that thermodynamics has a prominent effect on the morphology of the product.

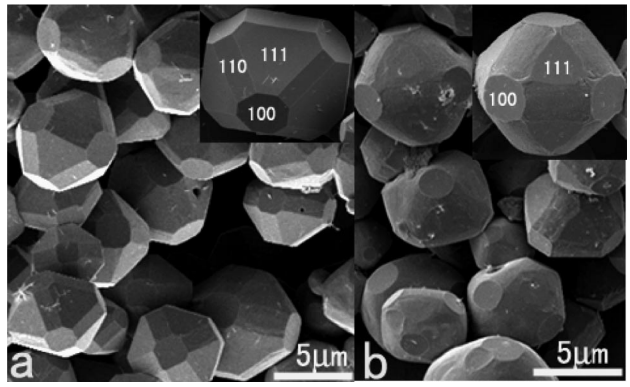

Figure 6. FE-SEM images of samples prepared with $[Cu(AC)_2 \cdot H_2O]$ = 0.025 M, $[dmgH_2]$ = 0.05 M, and [NaOH] = 0.45 M at reaction temperatures of (a) 180 °C, (b) 200 °C. The insets are high magnification images.

X-ray photoelectron spectroscopy (XPS) is a surface-specific technique that was also used to study the oxidation states and the surface composition of the as-made samples. The core-level Cu2p photoemission spectra of the as-made samples are presented in Figure 7. It can be clearly observed that the Cu $2p_{3/2}$ peak occurs at 932.4 ± 0.1 eV, which is known to be characteristic of Cu_2O instead of CuO and Cu.[45] The satellite feature at the high binding energy side of the Cu $2p_{3/2}$ peak is absent in the spectra, which further confirms the absence of CuO on the surface of the Cu_2O microcrystals. Hence, X-ray diffraction of the samples do not show evidence of CuO and Cu phases, and it can be concluded that the as-made samples are highly pure.

The Cu_2O could be used in the photocatalytic degradation of organic dyes. As Cu_2O has a powerful adsorption for molecular O_2, the electrons accumulated on the facets of the Cu_2O crystal can be scavenged by adsorptive O_2 to yield O^{2-}, and O^{2-} further reacts with H_2O and electrons to

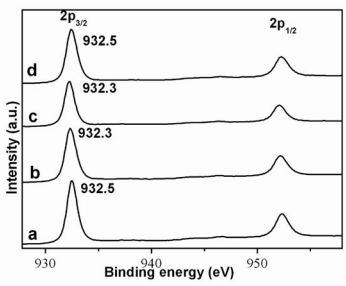

Figure 7. The core-level Cu2p XPS spectra of Cu_2O products with different morphologies: (a) porous hollow microspheres, (b) octahedral microcages with truncated corners and edges, (c) octahedral microcrystals with truncated corners and edges, (d) octahedral microcrystals.

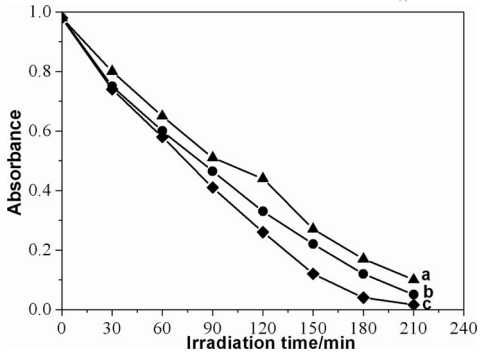

Figure 8. A plot showing the extent of photodegradation of rhodamine-B as a function of irradiation time for various samples: (a) octahedral microcrystals with truncated corners and edges, (b) octahedral microcrystals, and (c) octahedral microcages with truncated corners and edges.

produce hydrogen peroxide (H_2O_2) and the hydroxyl radical (·OH),[46] which can degrade most organic dyes. In our work, the synthesis of Cu_2O crystals with shape evolution provides an opportunity to examine their relative photocatalytic activity toward the degradation of organic dyes. We studied the optical property changes of rhodamine-B dyes irradiated by UV light in the presence of Cu_2O microcrystals. To demonstrate the structure–function correlation, three typical samples with comparable structure were studied: octahedra, octahedral microcages, and microcrystals with truncated corners and edges. As illustrated in Figure 8, octahedral Cu_2O microcrystal with entirely {111} surfaces ($0.25\ m^2 g^{-1}$) exhibited superior photoactivities over octahedral microcrystals with truncated corners and edges due to surface properties and not as a result of the higher surface area (Figure 8a,b). In fact, octahedral microcrystals with truncated corners and edges have a higher surface area ($0.41\ m^2 g^{-1}$). Huang reported that the {111} face of Cu_2O contains surface copper atoms with dangling bonds so that the {111} faces are higher in surface energy, and they expected to be more catalytically active than the {100} faces.[47–49] Thus, octahedral Cu_2O microcrystals with entirely {111} surfaces are more effective at photocatalysis reactions than microcrystals of other shapes containing partial {100} and {110} surfaces. Octahedral microcages with truncated corners and edges are more effective at photocatalysis reactions than particles with other shapes (Figure 8c). This can be attributed to the cavity structure, partial {111} surfaces, and the higher surface area ($1.71\ m^2 g^{-1}$). The cavity structure can allow the appearance of multiple reflections of light within the interior cavities and lead to the more efficient use of light and improve the photocatalytic activity of Cu_2O. Due to the very slow photocorrosion rate of the Cu_2O microcrystals, it is expected that these microcrystals with different surfaces may find more applications in photocatalysis.

Figure 9 shows the UV/Vis diffuse reflectance spectra of Cu_2O products with different morphologies including octahedra and octahedral microcages and microcrystals with truncated corners and edges. Intercepting the two linearly extrapolated lines, we can estimate the band gaps of Cu_2O according to the absorption edge positions. The optical absorption edges of octahedra and octahedral microcages and microcrystals with truncated corners and edges occurs at about 652, 645, and 646 nm, respectively, corresponding to a band gap energy of 1.90, 1.92, and 1.92 eV, respectively. The UV/Vis diffuse reflectance spectra indicates that the Cu_2O microcrystals are sensitive to ultra-visible light, which accounts for the photocatalytic activity of Cu_2O powders under ultra-visible light irradiation although it is not the only factor.

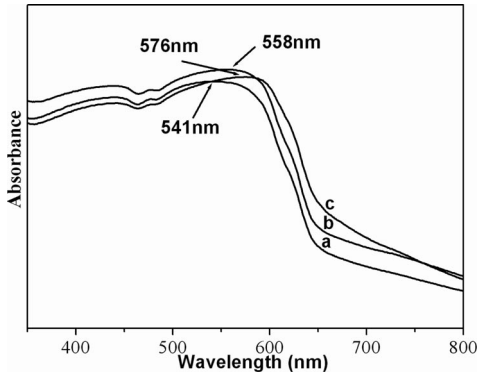

Figure 9. UV/Vis diffuse reflectance spectra of Cu_2O products with different morphologies: (a) octahedral microcages with truncated corners and edges, (b) octahedral microcrystals with truncated corners and edges, and (c) octahedral microcrystals.

Conclusions

A simple hydrothermal method has been successfully used to control the growth of the well-crystallized Cu_2O crystallites at a low temperature. Different morphologies of the Cu_2O crystallites can be easily obtained by varying temperature, reaction time, and concentration without any templates, surfactant, or other organic additives. On the basis of field emission scanning electron microscopy characterization analyses, a possible growth mechanism was proposed to explain the formation of various 3D architectures of the products. Rapid seed-particle aggregation, surface recon-

struction of the intermediate structure, and a solid core evacuation resulted in the growth of the microcages. To the best of our knowledge, this is the first time that this kind of Cu_2O microcages has been synthesized in this way. In addition, because of the various 3D architecture of the product, the samples can show different abilities to catalytically degrade rhodamine-B. It is believed that the controlled growth of Cu_2O crystals might bring many future potential applications in optical and electronic areas.

Experimental Section

Preparation of Cu_2O Microcrystals: All the reagents were of analytical grade and purchased from Shanghai Chemical. They were used as received without further purification. The synthesis of Cu_2O microcrystals was as follows: NaOH (0.5–2.0 g) and dimethylglyoxime (0.32 g, $dmgH_2$) were added into a 65-mL Teflon-lined stainless-steel autoclave, which was then filled with deionized water (55 mL), and the mixture was vigorously stirred. After complete dissolution of the dimethylglyoxime powder, $Cu(AC)_2{\cdot}H_2O$ (0.28 g) was added. The final aqueous solution concentrations were $[Cu(AC)_2{\cdot}H_2O]$ = 0.025 M, [NaOH] = 0.23–0.91 M, $[dmgH_2]$ = 0.05 M. After stirring for 4 h, the autoclave was maintained at 150–200 °C for 20 h and cooled down to room temperature naturally. The red products were collected and washed with distilled water, rinsed with ethanol, and then vacuum dried before characterization.

Photocatalytic Study: The photocatalytic activity of the Cu_2O powder was evaluated by the degradation of rhodamine-B under ultravisible light irradiation of a 200-W Hg lamp. In a typical process, Cu_2O (500 mg) was added to a rhodamine-B solution (45 mL, 1×10^{-5} M) and then magnetically stirred in the dark for 30 min, which allowed it to reach adsorption equilibrium, and then the solution was exposed to photoirradiation. Concentrations of rhodamine-B were carried out by using UV/Vis spectroscopy every 30 min.

Characterization: The products were characterized by X-ray power diffraction (XRD) by using a Philips X′pert X-ray diffractometer with Cu-K_α radiation (λ = 1.54187 Å). Field emission scanning electron microscopy (FE-SEM) image was taken with a Hitachi S-4800 scanning electron microanalyzer. Brunauere Emmette Teller (BET) surface areas were carried out by N_2 adsorption at 77 K by using the volumetric adsorption analyzer (ASAP 2010, Micromeritics Ins Corp.). X-ray photoelectron spectra (XPS) were measured by using a ESCALAB 250 with monochromated Mg-K_α irradiation. The UV/Vis absorption was recorded with a UV/Vis spectrophotometer Specord 200 (Analytic Jena AG) absorption diode array spectrometer by using 1-cm quartz curettes.

Acknowledgments

This project was financially supported by the National Science Foundation of China (Grant No. 10874161) and the National Basic Research Program of China (973 program, Grant No. 2009CB939901)

[1] Z. Wang, X. Chen, J. Liu, M. Mo, L. Yang, Y. Qian, *Solid State Commun.* **2004**, *130*, 585–589.
[2] G. Z. Mao, W. F. Dong, D. G. Kurth, H. Mohwald, *Nano Lett.* **2004**, *4*, 249–252.
[3] L. Ouyang, K. N. Maher, C. L. Yu, J. McCarty, H. Park, *J. Am. Chem. Soc.* **2007**, *129*, 133–138.
[4] Z. R. Dai, Z. W. Pan, Z. L. Wang, *Adv. Funct. Mater.* **2003**, *13*, 9–24.
[5] J. Q. Hu, Y. Bando, Q. L. Liu, D. Golberg, *Adv. Funct. Mater.* **2003**, *13*, 493–496.
[6] M. Maillard, S. Giorgio, M. P. Pileni, *J. Phys. Chem. B* **2003**, *107*, 2466–2470.
[7] Q. Peng, Y. J. Dong, Y. D. Li, *Angew. Chem. Int. Ed.* **2003**, *42*, 3027–3030.
[8] J. J. Zhu, S. Xu, H. Wang, J. M. Zhu, H. Y. Chen, *Adv. Mater.* **2003**, *15*, 156–157.
[9] B. Cao, Y. Jiang, C. Wang, W. Wang, L. Wang, M. Niu, W. Zhang, Y. Li, S. T. Lee, *Adv. Funct. Mater.* **2007**, *17*, 1501–1506.
[10] l. Andrew, A. L. Schmit, J. M. Higgens, S. Jin, *Nano Lett.* **2008**, *8*, 810–816.
[11] A. O. Musa, T. Akomolafe, M. J. Carter, *Sol. Energy Mater. Sol. Cells* **1998**, *51*, 305–316.
[12] R. N. Briskman, *Sol. Energy Mater. Sol. Cells* **1992**, *27*, 361–368.
[13] J. H. Li, B. X. Tang, L. M. Tao, Y. X. Xie, M. B. Zhang, *J. Org. Chem.* **2006**, *71*, 7488–7490.
[14] B. X. Tang, F. Wang, J. H. Li, Y. X. Xie, M. B. Zhang, *J. Org. Chem.* **2007**, *72*, 6294–6297.
[15] X. Li, H. Gao, C. J. Murphy, L. Gou, *Nano Lett.* **2004**, *4*, 1903–1907.
[16] R. Laskowski, P. Blaha, K. Schwarz, *Phys. Rev. B* **2003**, *67*, 075102–075110.
[17] Y. Chang, J. J. Teo, H. C. Zeng, *Langmuir* **2005**, *21*, 1074–1079.
[18] J. T. Zhang, J. F. Liu, Y. D. Li, *Chem. Mater.* **2006**, *18*, 867–871.
[19] M. Hara, T. Kondo, M. Komoda, S. Ikeda, K. Shinohara, A. Tanaka, J. Kondo, K. Domen, *Chem. Commun.* **1998**, *3*, 357–358.
[20] D. Snoke, *Science* **2002**, *298*, 1368–1372.
[21] P. He, S. X. Hen, H. Gao, *J. Colloid Interface Sci.* **2005**, *284*, 510–512.
[22] P. McFadyen, E. Matijevic, *J. Colloid Interface Sci.* **1973**, *44*, 95–98.
[23] Z. Z. Chen, E. W. Shi, Y. Q. Zheng, W. J. Li, B. Xiao, J. Y. Zhuang, *J. Cryst. Growth* **2003**, *249*, 294–300.
[24] C. Lu, L. Qi, J. Yang, X. Wang, D. Zhang, J. Xie, J. Ma, *Adv. Mater.* **2005**, *17*, 2562–2567.
[25] L. Gou, C. T. Murphy, *Nano Lett.* **2003**, *3*, 231–234.
[26] Z. Wang, X. Chen, J. Liu, M. Mo, L. Yang, Y. Qian, *Solid State Commun.* **2004**, *130*, 585–589.
[27] D. B. Wang, M. S. Mo, D. B. Yu, L. Q. Xu, F. Q. Li, Y. T. Qian, *Cryst. Growth Des.* **2003**, *3*, 717–720.
[28] H. G. Yu, J. G. Yu, S. W. Liu, S. Mann, *Chem. Mater.* **2007**, *19*, 4327–4334.
[29] C. H. Kuo, M. H. Huang, *J. Am. Chem. Soc.* **2008**, *130*, 12815–12820.
[30] European brewery Convention, Analytica EBC, 4th ed. [M], Brauerei und Getränke-Rundschau, Zürich, **1987**.
[31] Y. W. Jun, S. M. Lee, N. J. Kang, J. Cheon, *J. Am. Chem. Soc.* **2001**, *123*, 5150–5151.
[32] Y. H. Kim, W. Y. Jun, B. H. Jun, S. M. Lee, J. Cheon, *J. Am. Chem. Soc.* **2002**, *124*, 13656–13657.
[33] V. F. Puntes, D. Zanchet, C. K. Erdonmez, A. P. Alivisatos, *J. Am. Chem. Soc.* **2002**, *124*, 12874–12880.
[34] V. F. Puntes, K. M. Krishnan, A. P. Alivisatos, *Science* **2001**, *291*, 2115–2117.
[35] H. G. Yang, H. C. Zeng, *J. Phys. Chem. B* **2004**, *108*, 3492–3495.
[36] Y. Yin, R. M. Rioux, C. K. Erdonmez, S. Hughes, G. A. Somorjai, A. P. Alivisatos, *Science* **2004**, *304*, 711–714.

[37] S. H. Yu, B. Liu, M. S. Mo, J. H. Huang, X. M. Liu, Y. T. Qian, *Adv. Funct. Mater.* **2003**, *13*, 639–647.
[38] C. Jia, Y. Cheng, F. Bao, D. Q. Chen, Y. S. Wang, *J. Cryst. Growth* **2006**, *294*, 353–357.
[39] H. Wu, H. F. Xu, Q. Su, T. H. Chen, M. M. Wu, *J. Mater. Chem.* **2003**, *13*, 1223–1228.
[40] B. Liu, S. H. Yu, L. J. Li, Q. Zhang, F. Zhang, K. Jiang, *Angew. Chem. Int. Ed.* **2004**, *43*, 4745–4750.
[41] Y. W. Jun, J. H. Lee, J. S. Choi, J. Cheon, *J. Phys. Chem. B* **2005**, *109*, 14795–14806.
[42] X. M. Wang, H. Y. Xu, H. Wang, H. Yan, *J. Cryst. Growth* **2005**, 254–261.
[43] C. J. Murphy, *Science* **2002**, *298*, 2139.
[44] Z. L. Wang, *J. Phys. Chem. B* **2000**, *104*, 1153–1175.
[45] J. F. Moulder, W. F. Stickle, P. E. Sobol, K. D. Bomben in *Handbook of X-ray Photoelectron Spectroscopy*, Physical Electronic, Inc., USA, **1995**, p. 86.
[46] L. Huang, F. Peng, H. Yu, H. J. Wang, *Solid State Sci.* **2009**, *11*, 129–138.
[47] C. H. Kuo, C. H. Chen, M. H. Huang, *Adv. Funct. Mater.* **2007**, *17*, 3773–3780.
[48] C. H. Kuo, M. H. Huang, *J. Phys. Chem. C* **2008**, *112*, 18355–18360.
[49] J. Y. Ho, M. H. Huang, *J. Phys. Chem. C* **2009**, *113*, 14159–14164.

Received: September 2, 2009
Published Online: January 25, 2010

